Electronic Supplementary Material (ESI) for Journal of Materials Chemistry C.

Supplementary Information

Sub-10 nm Copper Chromium Oxide Nanocrystals As Solution Processed P-Type Hole Transport Layer For Organic Photovoltaics

Jian Wang, Yun-Ju Lee, Julia W. P. Hsu*

Department of Materials Science & Engineering, The University of Texas at Dallas, Richardson, TX

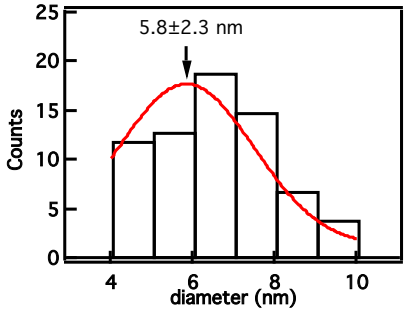

Figure S1. Histogram of individual $CuCrO_2$ nanocrystal size (measured from TEM images).

Figure S1 shows the histogram of individual $CuCrO_2$ nanocrystal sizes measured from transmission electron microscopy (TEM) images. A Gaussian fit shows that the averaged crystalline size is 5.8 ± 2.3 nm.

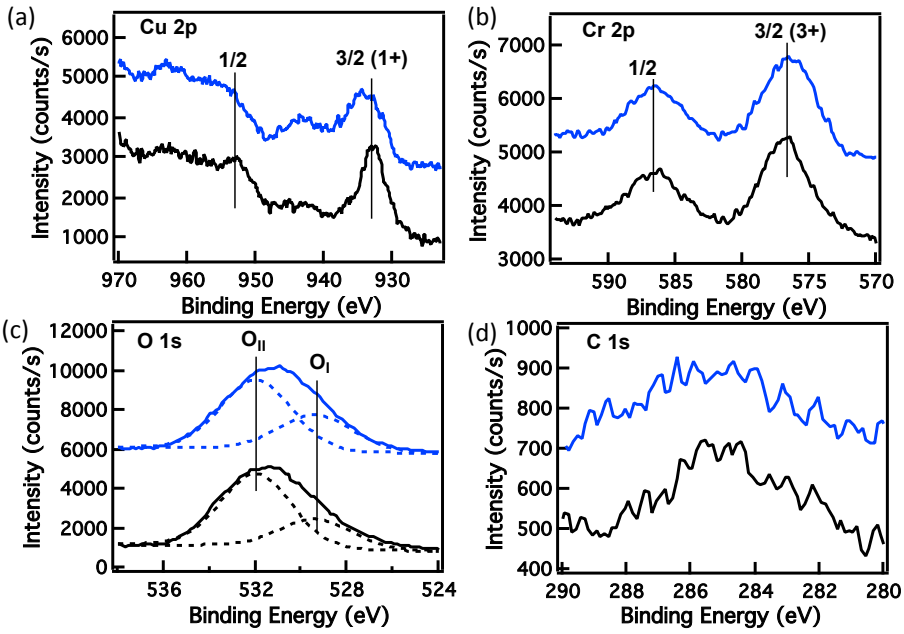

Figure S2. XPS spectra of (a) Cu 2p, (b) Cr 2p, (c) O 1s, and (d) C 1s, for as prepared $CuCrO_2$ film (black) or UV-ozone treated $CuCrO_2$ film (blue).

Figure S2 shows the X-ray photoelectron spectroscopy (XPS) of both as prepared and UV-ozone treated $CuCrO_2$ films on a gold substrate (to avoid oxygen signals from substrate). As discussed in main text, the Cu 2p 3/2 and Cr 2p 3/2 peaks are located at 932.7 eV and 576.7 eV, respectively, which are consistent with previous reported binding energies of Cu^{1+} and Cr^{3+} in $CuCrO_2$.[1] The O 1s are fitted into two species: the lattice oxygen in bulk $CuCrO_2$ at 529.3 eV (O_I), and the dissociated oxygen or hydroxyl species on surface at 532.0 eV (O_{II}).[2,3] The atomic ratio of Cu:Cr is determined as 0.6:1 from the as prepared $CuCrO_2$ film according to $\frac{AREA_{Cu\,2p}}{ASF_{Cu\,2p}} : \frac{AREA_{Cr\,2p}}{ASF_{Cr\,2p}}$, where the AREA is the total peak area, and ASF is the atomic sensitivity factor of corresponding Cu 2p and Cr 2p signal. After UV-ozone treatment, intensities and binding energies of all elements stay the same except for Cu 2p (Data fit is shown in Figure 7b main text). To determine the

ratio of Cu^{1+}, Cu^{2+}, and $Cu(OH)_2$ species in UV-ozone treated $CuCrO_2$ film, we correct the intensities of Cu^{2+} and $Cu(OH)_2$ species with their contribution to the area of Cu^{2+} satellites. For example, the peak area of Cu^{2+} satellite, $Cu(OH)_2$, Cu^{2+}, and Cu^{1+} are denoted as $AREA_{Cu\,SL}$, $AREA_{Cu(OH)_2}$, $AREA_{Cu^{2+}}$, and $AREA_{Cu^{1+}}$, respectively. After satellite area correction, the peak areas of Cu^{2+} and $Cu(OH)_2$, i.e. $AREA^c_{Cu^{2+}}$ and $AREA^c_{Cu(OH)_2}$, are calculated as

$$AREA^c_{Cu^{2+}} = AREA_{Cu^{2+}} + AREA_{Cu\,SL} \times \frac{AREA_{Cu^{2+}}}{AREA_{Cu^{2+}} + AREA_{Cu(OH)_2}}, \text{ and}$$

$$AREA^c_{Cu(OH)_2} = AREA_{Cu(OH)_2}, + AREA_{Cu\,SL} \times \frac{AREA_{Cu(OH)_2},}{AREA_{Cu^{2+}} + AREA_{Cu(OH)_2}}, \text{ respectively.}$$

Finally, the ratio of Cu^{1+}, Cu^{2+}, and $Cu(OH)_2$ species is calculated by $AREA_{Cu^{1+}} : AREA^c_{Cu^{2+}} : AREA^c_{Cu(OH)_2}$.

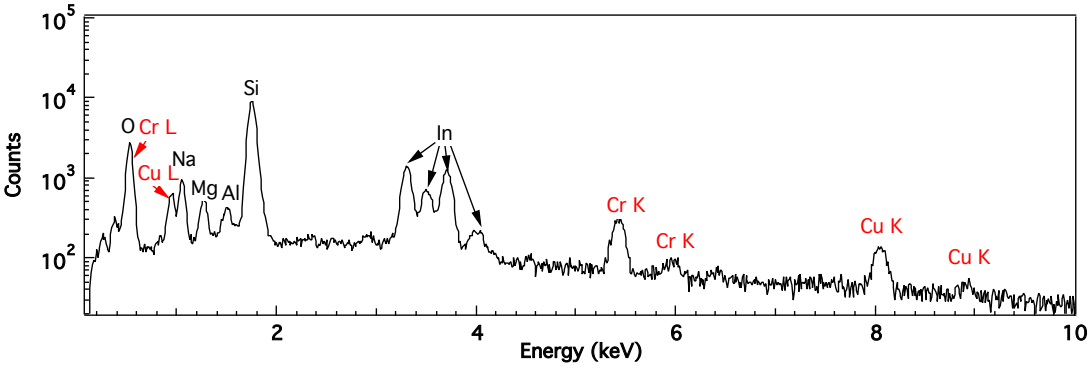

Figure S3. EDAX spectra of $CuCrO_2$ film on an ITO/glass substrate. Elements labeled in black fonts are from substrates.

Figure S3 shows the energy dispersive X-ray spectroscopy (EDAX) spectrum of a $CuCrO_2$ film on ITO/glass substrate. The signals of Na, Al, Mg, Si, and In are from substrate. The O signal is also mostly from the ITO/glass substrate, hence cannot be used to deduce the oxygen ratio in $CuCrO_2$. Since the Cr L signal overlaps with the O signal,

we use the Cu K signal and Cr K signal to determine their atomic ratio, which is 0.85:1. Based on the discussion in main text, given these $CuCrO_2$ nanocrystals have surface Cr oxide layers, it is reasonable that the surface-sensitive XPS observes a lower Cu:Cr ratio than the bulk-sensitive EDAX.

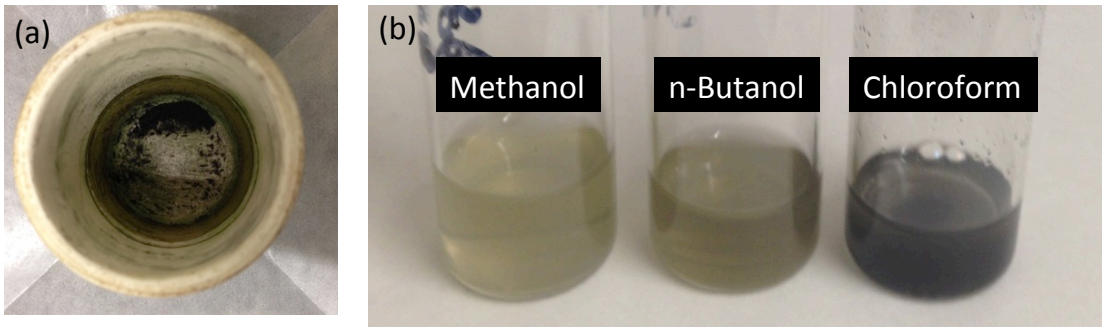

Figure S4. Photographs of (a) $CuCrO_2$ powder, and (b) $CuCrO_2$ suspensions in selected solvents.

Figure S4(a) shows the dark green $CuCrO_2$ powders in a crucible. Figure S4(b) shows three $CuCrO_2$ suspensions in solvents with different polarity. In a polar solvent (methanol), the suspension is translucent light green, whereas in a nonpolar solvent (chloroform), the suspension is dark green. DLS measurement shows that the hydrodynamic size of $CuCrO_2$ is on the order of μm when suspension is dark green, indicating a poor dispersion. Other solvents such as ethanol, isopropanol, acetone, acetonitrile, toluene, pyridine, chlorobenzene, and 2-methoxyethanol are also examined.

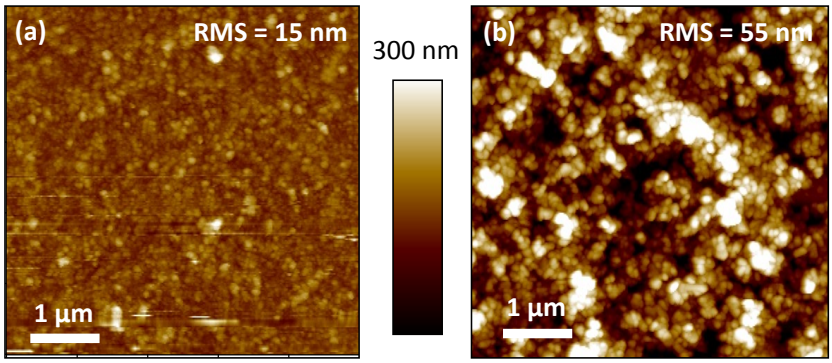

Figure S5. AFM images of (a) ~ 30 nm $CuCrO_2$ film, and (b) ~ 280 nm $CuGaO_2$ film.

Figure S5 shows the AFM image comparison between the $CuCrO_2$ film and $CuGaO_2$ film. It is clear that the $CuCrO_2$ film is much smoother than $CuGaO_2$ film (root-mean-square RMS roughness 15 nm vs. 55 nm). The $CuCrO_2$ film is ~ 30 nm thick as determined from ellipsometry, while $CuGaO_2$ film is ~ 280 nm according to AFM. Note that these two films are at the smallest thicknesses that warrant a continuous film for either $CuCrO_2$ or $CuGaO_2$ nanocrystals. Also, the light transmission through these two films is similar (> 90%). Therefore, the morphology comparison is relevant since devices are made on top of such films.

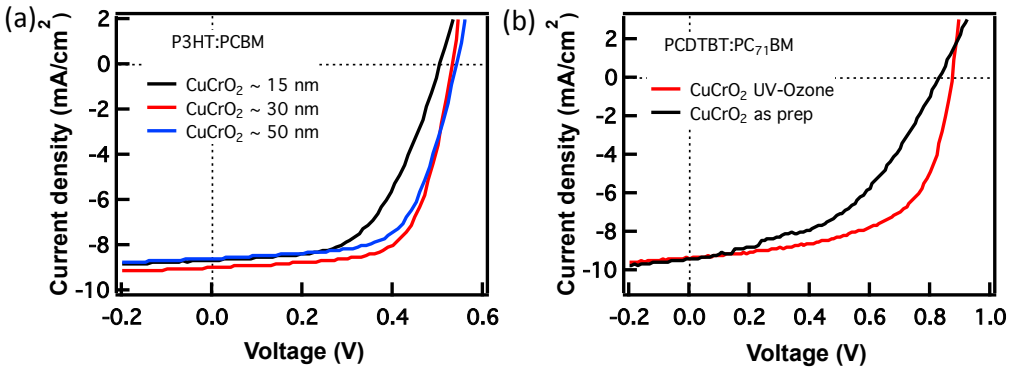

Figure S6. *J-V* characteristics under AM 1.5G 100 mW/cm^2 illumination of (a) P3HT:PCBM devices with different $CuCrO_2$ (UV-Ozone treated) thicknesses, and (b) PCDTBT:$PC_{71}BM$ devices with ~ 30 nm as prepared or UV-Ozone treated $CuCrO_2$ HTL.

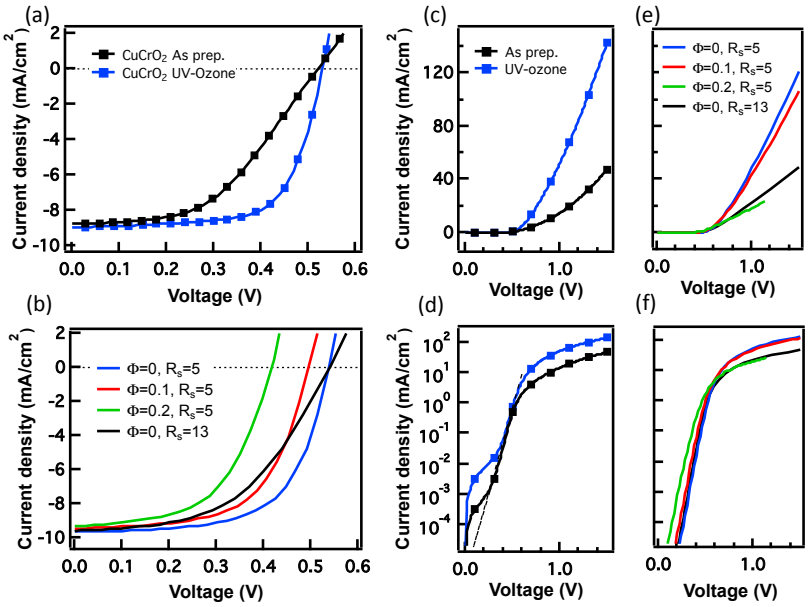

Figure S7. *J-V* characteristics of P3HT:PCBM devices under AM 1.5G 100 mW/cm^2 illumination (a)-(b), and in dark (c)-(f). (a), (c), (d) are experimental results, and (b), (e), (f) are SCAPS simulated results. (c) and (d), or (e) and (f), are the same data plotted either in linear-linear scale or log-linear scale.

Figure S7 shows the comparison between experimental *J-V* results (same as Figure 6 in main text) and drift-diffusion simulated *J-V* results. In the drift-diffusion simulation, the anode injection barrier and series resistance are varied, while the rest parameters are kept constant and listed below.[5] The simulation with 0.2 eV anode injection barrier and 5 Ω cm^2 series resistance (green line) failed to converge beyond 1.1 V bias. Although increasing injection barrier Φ from 0 eV (blue line), to 0.1 eV (red line), and to 0.2 eV (green line) decreases device fill factor (*FF*) and injection current in dark, it also decreases device open-circuit voltage (V_{oc}) and turn-on voltage in dark, which is not seen in experimental results. On the other hand, simply adding a 13 Ω cm^2 series resistance (black line) in simulation leads to very similar (both light and dark) *J-V* curves as the experimental results. This simulation confirms the formation of Ohmic contact at hole transport layer/active layer interface for both as prepared and UV-ozone treated $CuCrO_2$

films, indicating that the performance of device with as prepared $CuCrO_2$ HTL is limited by an internal resistance.

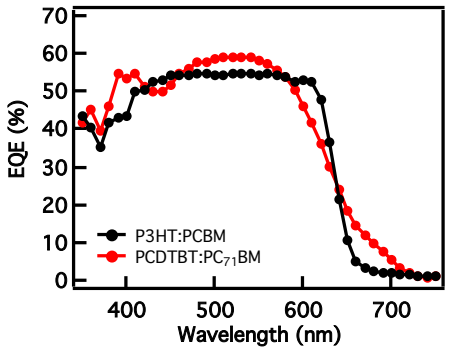

Figure S8. External quantum efficiency (EQE) measurement of P3HT:PCBM and PCDTBT:PC_{71}BM devices with ~ 30 nm UV-Ozone treated $CuCrO_2$ HTL. The integrated photocurrents are 8.3 mA/cm^2 and 8.7 mA/cm^2, respectively, consistent with J_{sc} values obtained in *J-V* measurement (Table 1&2 in main text).

Table S1. Parameters used for drift-diffusion simulation. Except the anode injection barrier and series resistance (red font), the rest parameters are adopted from reference 5.

Active Layer Thickness (nm)	210
Dielectric Permittivity	3.8
Electron Affinity (eV)	3.7
Effective Bandgap (eV)	1.0
Cathode injection barrier (eV)	0.1
Anode injection barrier (eV)	0 or 0.1 or 0.2
Bimolecular Recombination Coefficient (cm^3/s)	1.0 E -12
Surface Recombination Velocity (cm/s)	1.0 E +5
CB & VB Effective Density of States (cm^{-3})	1.0 E +20
Electron Mobility (cm^2/Vs)	2.5 E -3
Hole Mobility (cm^2/Vs)	5.0 E -4
Doping Concentration N_A (cm^{-3})	1 E +16
Series resistance (Ω cm^2)	5 or 13

References

1 M. Han, K. Jiang, J. Zhang, W. Yu, Y. Li, Z. Hu and J. Chu, *J. Mater. Chem.*, 2012, **22**, 18463.

2 C. D. Wagner, W. M. Riggs, L. E. Davis, J. E. Moulder and G. E. Muilenberg, *Handbook of X-ray Photoelectron Spectroscopy*, 1st ed.; Perkin-Elmer Corporation: Waltham, MA, 1979.

3 E. L. Ratcliff, J. Meyer, K. X. Steirer, A. Garcia, J. J. Berry, D. S. Ginley, D. C. Olson, A. Kahn and N. R. Armstrong, *Chem. Mater.*, 2011, **23**, 4988–5000.

4 A. P. Amrute, Z. Łodziana, C. Mondelli, F. Krumeich and J. Pérez-Ramírez, *Chem. Mater.*, 2013, **25**, 4423–4435.

5 J. Wang, L. Xu, Y.-J. Lee, M. De Anda Villa, A. V. Malko and J. W. P. Hsu, *Nano Lett.*, 2015, **15**, 7627–7632.